Catalysis Today 224 (2014) 147–153

Contents lists available at ScienceDirect

Catalysis Today

journal homepage: www.elsevier.com/locate/cattod

# $Bi_2WO_6$/PANI: An efficient visible-light-induced photocatalytic composite

Wenzhong Wang*, Jiehui Xu, Ling Zhang, Songmei Sun

*State Key Laboratory of High Performance Ceramics and Superfine Microstructure, Shanghai Institute of Ceramics, Chinese Academy of Sciences, 1295 Dingxi Road, Shanghai 200050, PR China*

ARTICLE INFO

*Article history:*
Received 31 July 2013
Received in revised form 23 October 2013
Accepted 1 November 2013
Available online 9 December 2013

*Keywords:*
$Bi_2WO_6$
Polyaniline
Photocatalytic film
Visible light

ABSTRACT

$Bi_2WO_6$ photocatalyst film prepared by a facile chemical bath deposition (CBD) method was modified by polyaniline (PANI) through in situ polymerization of vapor phase aniline. The photocatalytic activities of the PANI/$Bi_2WO_6$ film were evaluated by the degradation of a widely used dye, tetraethylated rhodamine (RhB), and a general gaseous indoor air pollutant, acetaldehyde under visible-light irradiation ($\lambda > 420$ nm). The excellent performance of the PANI/$Bi_2WO_6$ film could be attributed to the rapid separation and slow recombination of the photogenerated electron–hole pairs contributed by the synergic effect between PANI and $Bi_2WO_6$. The stability of the photocatalytic film is found to be satisfying, which makes it potential in practical application. This work not only solves the separation and recycling problem for nano-sized photocatalyst, but also provides insight into the design of photocatalytic film with high activity for environmental applications, especially for indoor air purification.



## 1. Introduction

Photocatalysis is considered as a promising technique for the purification of polluted water and air. With the increasing demand of directly utilizing solar energy, the development of visible light responsive photocatalyst is becoming one of the goals in the research of photofunctional materials. $Bi_2WO_6$, with a band gap of 2.6–2.8 eV, has exhibited relatively high efficiency in the visible light induced photocatalyst for mineralizing organic contaminants (apparent quantum efficiency under 400 nm irradiation, ~8%) without any surface modification [1]. Recently, it has been extensively investigated as a potential visible light induced photocatalyst [2–5]. However, few studies were focused on the preparation of films which is beneficial for practical photocatalytic application. And the film deposition methods mainly fasten on the dip-coating method for its easy processing [6–9]. To achieve better adherence to the substrate, for the first time, we deposited $Bi_2WO_6$ photocatalyst with well-defined morphology on stainless steel mesh through a chemical bath deposition (CBD) method.

For photocatalytic films, the significant loss of active sites on the surface of the photocatalyst limits its efficiency in the photocatalytic degradation of pollutants. Our previous work has reported a way to improve it by developing new kind of reticular stainless steel mesh substrate with large surface area [9]. The as-prepared $Bi_2WO_6$ film possesses notable advantages in the decomposition of gaseous contamination especially in static system. The interface between the photocatalyst and contaminant was increased because the $Bi_2WO_6$ particles were well dispersed on the substrate with high surface area, rather than agglomerated together in the static degradation system of photocatalyst powders. To improve the photocatalytic activity further, promotion of the separation efficiency of photogenerated electron–hole pairs is considered to be one of the most effective ways [10]. Coupling with materials of delocalized conjugated structures is such an efficient approach, because rapid photoinduced charge separation and relatively slow charge recombination in electron-transfer processes were realized [11]. In particular, polyaniline (PANI), as one of the most important intrinsically conducting polymers (ICPs) with an extended $\pi$-conjugated electron system, has recently showed great promises due to its high absorption coefficients in the visible-light range and high mobility of charge carriers [12]. Taking account of the efficient carrier-transfer property of PANI, it is expected that the coupling of photocatalyst and PANI would be ideal for enhancing the activity under visible light. As reported, however, most of photocatalysts were coupled with PANI through a simple dipping procedure [13–15]. Although it is convenient since no further treatment was involved, the adherence between PANI and substrate through physical adsorption is not firm enough. Several groups reported the deposition of ICP layers by in situ polymerization techniques, where the substrate materials were successively coated by oxidant and monomer layers, in solution or vapor phase [16–20]. This flexible method essentially allows the addition of electronic

* Corresponding author. Tel.: +86 21 5241 5295; fax: +86 21 5241 3122.
*E-mail address:* wzwang@mail.sic.ac.cn (W. Wang).

0920-5861/$ – see front matter © 2013 Elsevier B.V. All rights reserved.
http://dx.doi.org/10.1016/j.cattod.2013.11.030

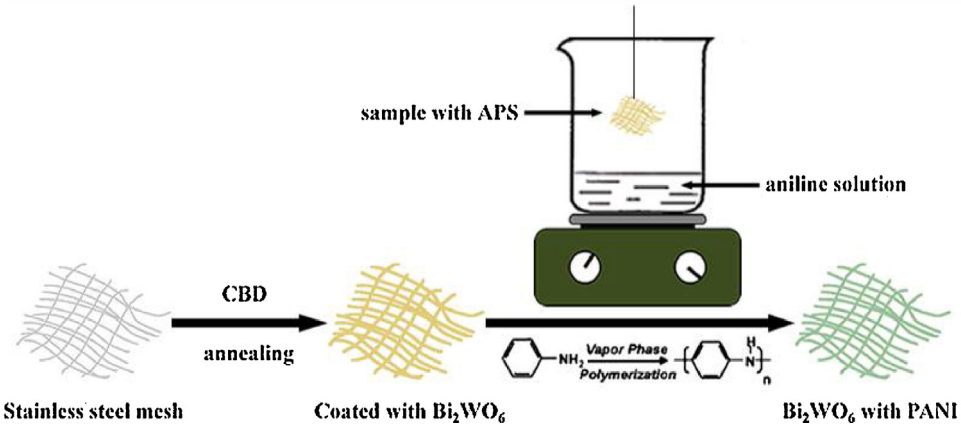


**Scheme 1.** The process of in situ polymerization of PANI on $Bi_2WO_6$ film by CBD method.

properties to film (with optimized mechanical properties) using standard coating procedures.

In this study, the $Bi_2WO_6$ photocatalyst film prepared by CBD method was modified with PANI by vapor-phase techniques. The PANI coating process was realized by an in situ polymerization instead of dipping procedure. The photocatalytic activity and stability of as-prepared PANI/$Bi_2WO_6$ film were evaluated by the degradation of contaminants in aqueous/gaseous phases under visible irradiation ($\lambda > 420$ nm). Moreover, we aimed to approach the possible mechanism of the improved activity in order to guide further work for the improvement of photocatalytic performance.

## 2. Experimental

### 2.1. Preparation of PANI/$Bi_2WO_6$ film

All the chemicals were analytical grade reagents from Shanghai Chemical Company and used without further purification. $Bi_2WO_6$ film has been deposited on the substrate of twill weaved 400 meshes stainless steel mesh made of SUS 304 ($5 \times 5$ cm). Before deposition, the substrates were cleaned by sonication for 15 min in anhydrous ethanol and dilute hydrochloric acid (1 wt.%) respectively and then rinsed with deionized water. In a typical procedure, $Bi(NO_3)_3{\bullet}5H_2O$ and $Na_2WO_4{\bullet}2H_2O$, in a molar ratio of 2:1, were dissolved in the mixed solvent of ethylene glycol (EG) and 2-methoxyethanol (2-MOE), in a volume ration of 1:3. The concentrations of $Bi_2WO_6$ in the bulk solution ranged from 5 to 12.5 mmol/L (mM). The pre-treated substrates were immersed in the above solution for about 1 h to facilitate nucleation on the substrate surface [21], and then the solution was refluxed at 120 °C for 12 h. Afterwards, the film and particles in the solution were collected, rinsed with anhydrous ethanol and deionized water, and then oven-dried at 60 °C. For better crystallization, the obtained film and particle samples were thermal treated at 450 °C for 1 h in air.

The PANI coating process is described in Scheme 1. The annealed CBD films were dipped into an ammonium persulfate (APS) solution. 2% (v/v) of concentrated HCl was added to the oxidant solution in order to obtain the acid doping PANI coating layer which is conductive. Excess APS solution was wiped off. The films were then transferred into a reactor which was heated by hot plate at 40 °C to make the monomer solution of aniline evaporate. The monomer vapors polymerized when they came in contact with the APS-coated films, producing a thin PANI coating, doped with $H^+$ ions. The polymerization time was set as 1 h. Afterwards, the obtained film was collected and rinsed with anhydrous ethanol and deionized water and then oven-dried at 60 °C.

### 2.2. Characterization of PANI/$Bi_2WO_6$ photocatalytic film

The purity and crystallinity of the as-prepared $Bi_2WO_6$ powders and films were characterized by powder X-ray diffraction (XRD) with a Rigaku D/MAX 2250 V diffractometer using monochromatized Cu Kα ($\lambda = 0.15418$ nm) radiation under 40 kV and 100 mA and scanning over the range of $20° \leq 2\theta \leq 70°$. The morphologies and microstructures characterizations were performed on the scanning electron microscope (SEM, JEOL JSM-6700F). UV–vis diffuse reflectance spectra (DRS) of the samples were obtained on an UV–vis spectrophotometer (Hitachi U-3010) using $BaSO_4$ as the reference.

Photocatalytic activities of the samples were evaluated by the degradation of model contaminants under the irradiation of a 500 W Xe lamp with a 420 nm cutoff filter. For the decolorization of RhB, 0.1 g of $Bi_2WO_6$ photocatalyst was added into 100 mL of RhB solution ($10^{-5}$ mol/L) and stirred in the dark for 2 h before illumination to ensure the establishment of an adsorption–desorption equilibrium between the photocatalyst and RhB. For the $Bi_2WO_6$ film samples, they were placed into 50 mL of RhB solution ($10^{-5}$ mol/L) and kept in the dark for 2 h to ensure the adsorption–desorption equilibrium. At 10 min or 30 min intervals, the absorption of a 3 mL of sample solution was recorded on a Hitachi U-3010 UV–vis spectrophotometer. For the degradation of acetaldehyde ($CH_3CHO$), the film was placed at the bottom of a gas-closed reactor with a quartz window at room temperature (capacity 600 mL). The reaction gas mixture (1 atm) consisted of 100 ppm $CH_3CHO$ and $N_2$ balance gas. Prior to irradiation, the reaction system was equilibrated for about 30 min until no change in the concentration of $CO_2$ was monitored. Gaseous samples (1 mL) were periodically extracted and analyzed by a gas chromatograph (GC) equipped with a flame ionization detector ($N_2$ carrier) and a catalytic conversion furnace.

## 3. Results and discussion

As a one-step, low-energy-consumption technique, chemical bath deposition (CBD) has been widely applied for depositing large-area films with particular shape, orientation and thickness [22,23], in which thin films are deposited on the substrates immersed in dilute solutions. This process is on the base of the controlled precipitation of the metal ion in the reaction bath. Many metal chalcogenide (including sulfides, selenides) and simple metal oxides thin films have been prepared by CBD [24–26]. However, multiple metal oxide functional films were rarely deposited through this process. This could be ascribed to the critical phase formation temperature of the multiple metal oxides which is mainly

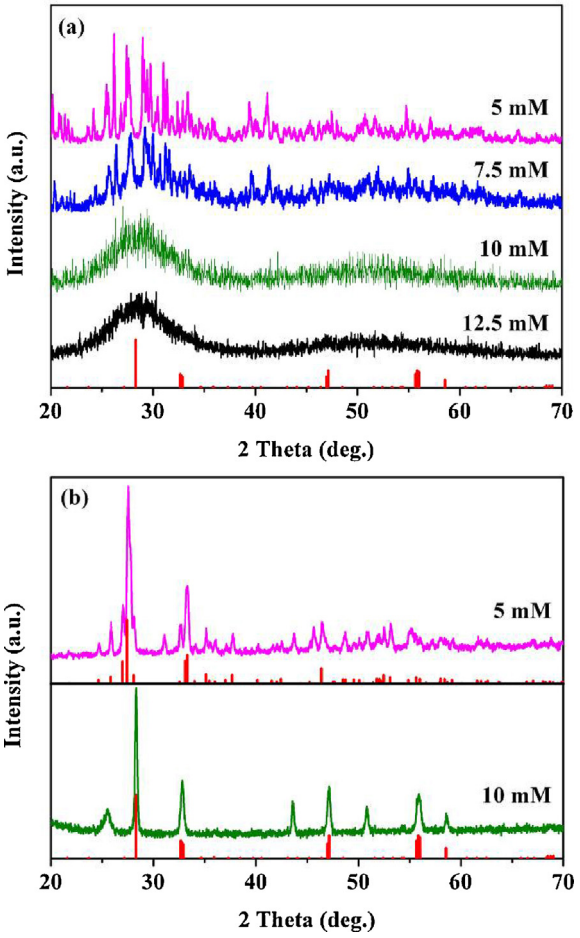


**Fig. 1.** XRD patterns of the $Bi_2WO_6$ powders by CBD process at different concentrations (a) and the calcinated films at the concentration of 5 and 10 mM (b).

higher than those of the metal chalcogenide. Moreover, spontaneous precipitation of $Bi_2WO_6$ occurs when aqueous solutions containing salts of $Bi^{3+}$ and $WO_4^{2-}$ are mixed which will lead to the formation of large particles. This procedure yields particles without morphology control resulting in bad adherence to the substrates, which favors the formation of dispersed particles rather than being deposited on the substrates. In order to prepare $Bi_2WO_6$ particles with well-defined morphology, the reaction conditions should be well controlled so as to the nucleation and growth of the solid [27]. Herein, the mixed solvent of ethylene glycol (EG) and 2-methoxyethanol (2-MOE) was utilized to prevent the hydrolysis of $Bi^{3+}$ and avoid the spontaneous precipitation of $Bi^{3+}$ and $WO_4^{2-}$, via the unique coordination of EG and 2-MOE. Compared to pure solvent of EG, the mixed solvent containing 2-MOE not only decrease the refluxing temperature because of its low boiling point, but also maintain the coordination with $Bi^{3+}$ and $WO_4^{2-}$.

The influence of initial concentration of the precursor (5, 7.5, 10, and 12.5 mM) on the formation of $Bi_2WO_6$ phase was checked. The phase and composition of the $Bi_2WO_6$ particles collected after the deposition process were given in Fig. 1a. At lower concentrations (5 and 7.5 mM), the peaks were weak with noisy background while they were identified as some intermediate products such as ammonium tungstate. While at higher concentration (10 and 12.5 mM), although the product was poorly crystallized, the XRD pattern can be indexed to orthorhombic $Bi_2WO_6$ (JCPDS 39-0256). The calcination process favors the formation of good crystallization, and the diffraction peaks of calcined films were demonstrated in Fig. 1b. As shown, at the concentration of 5 mM, the diffraction peaks agree well with those of the monoclinic phased $Bi_2O_3$ according to the JCPDS 65-2366, accompanied by the diffraction of the stainless steel substrate. In contrast, the film deposited at higher concentration of 10 mM matched well with orthorhombic $Bi_2WO_6$, again, except for the peaks of substrate. The diffraction profiles reveal that $Bi_2WO_6$ are well crystallized after calcination and the broad diffraction peaks imply that the crystalline grains are on nanoscale.

To further investigate the influence of concentration on the morphological evolution process of the $Bi_2WO_6$ film, a series of SEM images of calcined films obtained at different concentrations were revealed in Fig. 2. As it has been verified that $Bi_2WO_6$ phase can only be obtained at higher concentration, the particles differed in size and shape. At lower concentration, $Bi_2O_3$ particles were obtained and they were smaller and closely packed into larger agglomerates. They tended to aggregate on bent parts of stainless steel wire with high surface energy instead of uniformly coat on the whole part of the wire (Fig. 2a–d). While at higher concentration, the size distribution of $Bi_2WO_6$ particles was uniform consisting of spheres with a diameter of 400–500 nm. Higher concentration favored to form larger particles and thicker coating layers (Fig. 2g and h). As no surfactants were involved, these nanoparticles were quickly built and spontaneously aggregated to minimize their surface area through the process known as Ostwald ripening.

Photocatalytic degradation of RhB was performed under visible light irradiation ($\lambda > 420$ nm) to evaluate the photocatalytic properties of the $Bi_2WO_6$ powders and films. RhB, a representative textile dye, showed a major absorption band at 553 nm. Fig. 3 displays the temporal evolution of the spectral changes during the photodegradation of RhB by $Bi_2WO_6$ powders (a) and film (b) obtained at the concentration of 10 mM $Bi_2WO_6$ in the bulk solution. A decrease of RhB absorption at a wavelength of 553 nm was observed, along with absorption band shifts to shorter wavelengths. The destruction of the dye chromophore structure was induced by the predominant oxidation of the hydroxyl radicals (photogenerated holes) localized at the surface of irradiated photocatalyst [28]. Compared to the slurry system, the photocatalytic activity of $Bi_2WO_6$ film decreased dramatically. Nearly 100% of RhB was decolorized by the $Bi_2WO_6$ powders under visible light in 30 min, however, only 59% by $Bi_2WO_6$ film under the same condition. It took more than 3 h to decolorize 100% of RhB by the film. The immobilization of the photocatalyst led to significant reduction of the interface between the photocatalyst and contaminant, which remains the major obstacle in the application and popularization of photocatalysis technology.

For the significant loss in the activity in the photocatalytic degradation of pollutants because of the decrease of active sites on the surface of the photocatalyst, PANI was coupled to promote the separation efficiency of photogenerated electron–hole pairs. The in situ vapor-phase polymerization method was introduced on the surface of $Bi_2WO_6$ film. The polymerization of aniline was observed as the appearance of the film changed from yellowish to green. The diffuse-reflection spectra (DRS) of the $Bi_2WO_6$ and PANI/$Bi_2WO_6$ films are depicted in Fig. 4. The $Bi_2WO_6$ film sample exhibited photoabsorption from UV light to visible light, and the absorption edge locates at 450 nm. The absorption of the PANI/$Bi_2WO_6$ film sample increases over nearly the whole range of the spectrum. Therefore, the PANI-modified $Bi_2WO_6$ film can be excited to produce more electron–hole pairs under the same visible-light illumination, which could result in higher photocatalytic activity.

The photodegradation efficiency of RhB by PANI/$Bi_2WO_6$ film which is displayed in Fig. 5 verified the synergetic effect of PANI on the photocatalytic activity of $Bi_2WO_6$. As shown, the adsorption of RhB on the PANI/$Bi_2WO_6$ film is stronger than that on the $Bi_2WO_6$ film after 2 h in the dark. The concentration of RhB decrease obviously under the irradiation of visible light within 1.5 h, suggesting the decolorizing of RhB was photodegraded by PANI/$Bi_2WO_6$ film. Comparison of the photodegradation efficiency with pure

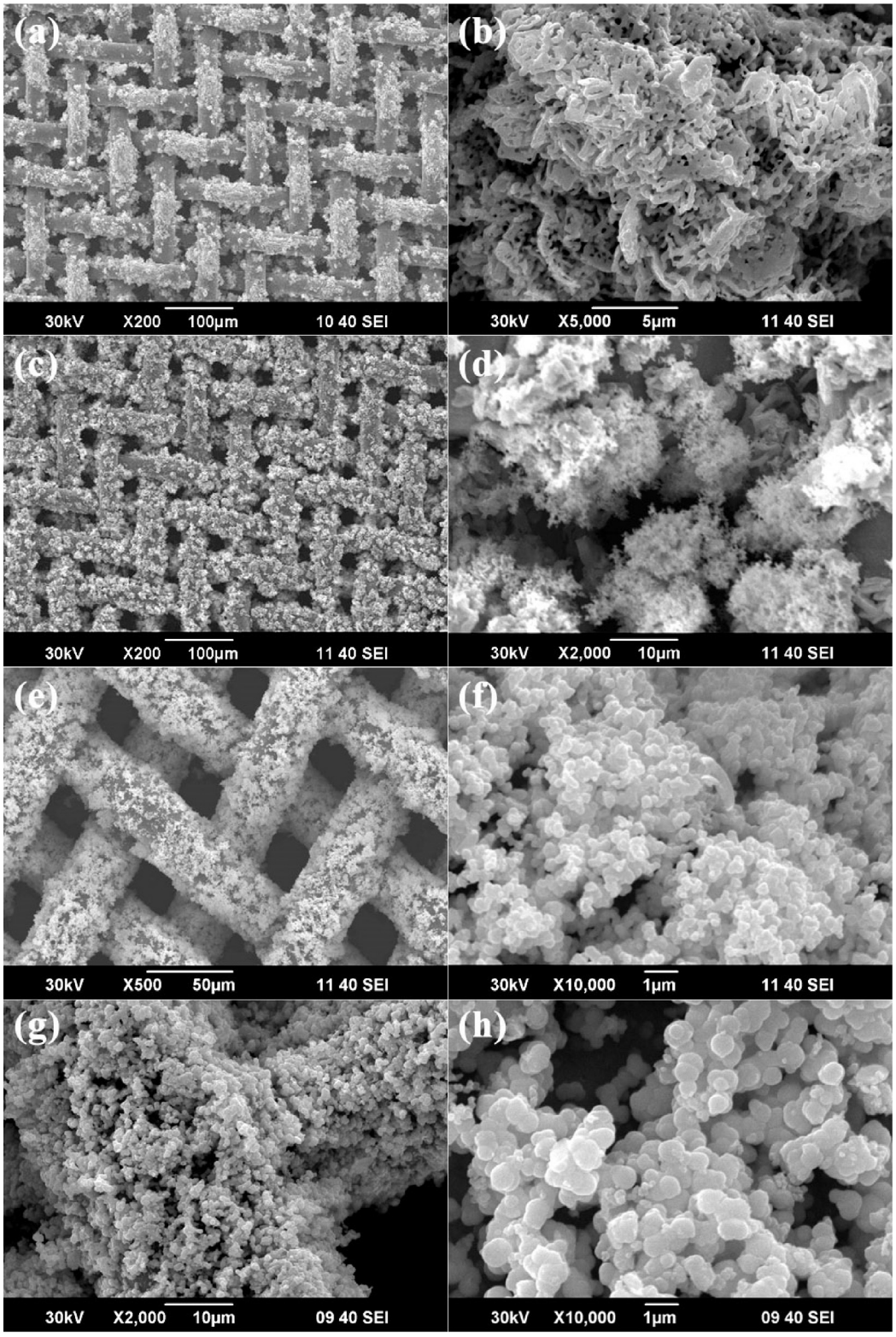


**Fig. 2.** SEM images of as-synthesized $Bi_2WO_6$ films by CBD process at different concentrations (from 5 mM to 12.5 mM) of low (a, c, e, g) and high (b, d, f, h) magnifications.

$Bi_2WO_6$ film is revealed in Fig. 5b, where $C$ is the concentration of RhB at the irradiation time $t$ and the $C_0$ is the initial concentration when the adsorption–desorption equilibrium between photocatalyst and RhB was established in dark. It was displayed that less than 80% RhB can be degraded by pure $Bi_2WO_6$ film under visible light in 1.5 h. Therefore, the PANI/$Bi_2WO_6$ film exhibited higher photodegradation efficiency with higher absorption capability compared with pure $Bi_2WO_6$ film.

Besides the enhanced photocatalytic activity resulting from PANI, the photostability of the photocatalyst was also retained [14]. The circulating runs in the photocatalytic degradation of RhB in the presence of PANI/$Bi_2WO_6$ film under visible light ($\lambda > 420$ nm)

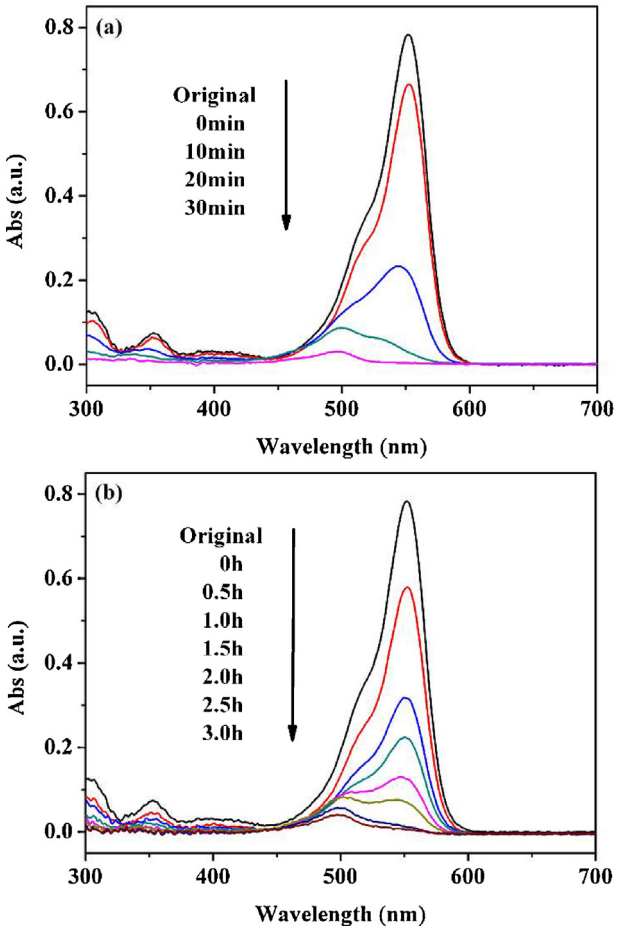


**Fig. 3.** RhB aqueous solution ($10^{-5}$ mol/L) degradation in the presence of the $Bi_2WO_6$ powders (a) and film (b) by CBD process at the concentration of 10 mM under visible-light irradiation ($\lambda > 420$ nm).

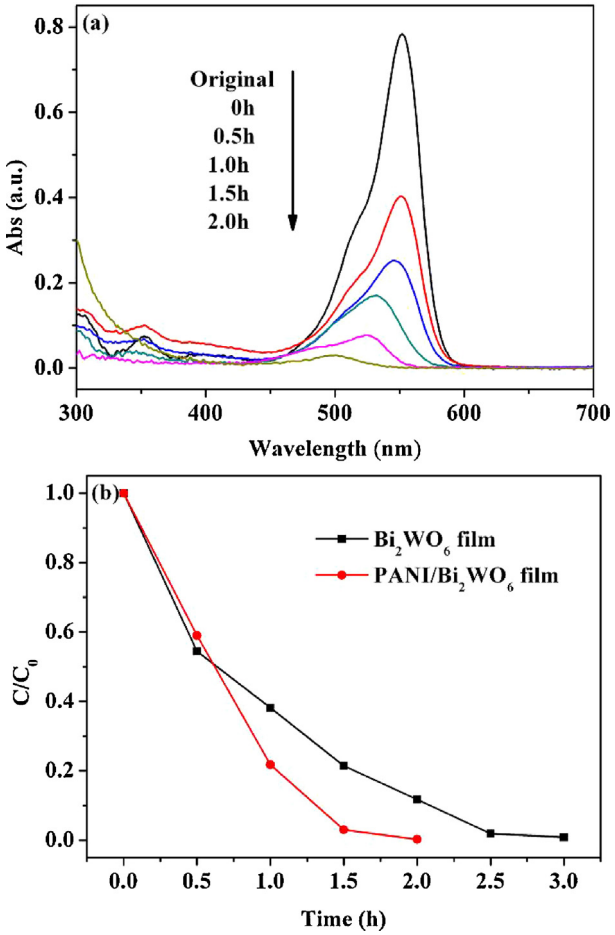


**Fig. 5.** RhB aqueous solution ($10^{-5}$ mol/L) degradation in the presence of the $PANI/Bi_2WO_6$ film (a) and the changes of temporal UV–vis spectral of RhB by $Bi_2WO_6$ and $PANI/Bi_2WO_6$ film under visible-light irradiation ($\lambda > 420$ nm).

were checked. Fig. 6 shows $C/C_0$ as a function of time, where $C$ is the concentration of RhB at the irradiation time $t$ and the $C_0$ is the initial concentration when the adsorption–desorption equilibrium between photocatalyst and RhB was established in dark. After five cycles for the photodegradation of RhB, the activity of the photocatalyst did not exhibit any significant loss. It indicates that the $PANI/Bi_2WO_6$ photocatalytic film has high stability and does not photocorrode during the photocatalytic oxidation of the model pollutant molecules. PANI is also cheaper than noble metals; thus, the $PANI/Bi_2WO_6$ photocatalytic film is promising for practical application in water purification.

To further confirm the photocatalytic properties of the as-prepared $PANI/Bi_2WO_6$ film and eliminate the photosensitive effect of RhB, gaseous acetaldehyde ($CH_3CHO$) was selected to evaluate the photocatalytic activity. Different from RhB, $CH_3CHO$

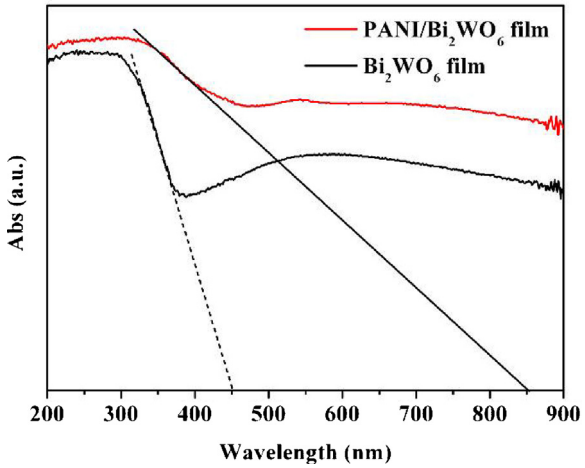


**Fig. 4.** UV–vis diffuse reflectance spectra of the as-synthesized $Bi_2WO_6$ and $PANI/Bi_2WO_6$ film.

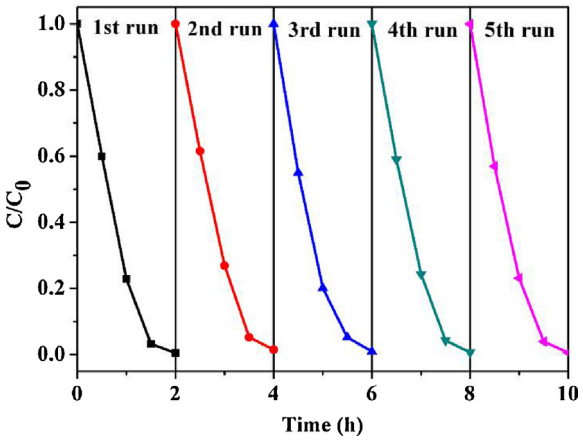


**Fig. 6.** Cycling experiment of the photocatalytic degradation of RhB in the presence of $PANI/Bi_2WO_6$ film under visible-light irradiation ($\lambda > 420$ nm).

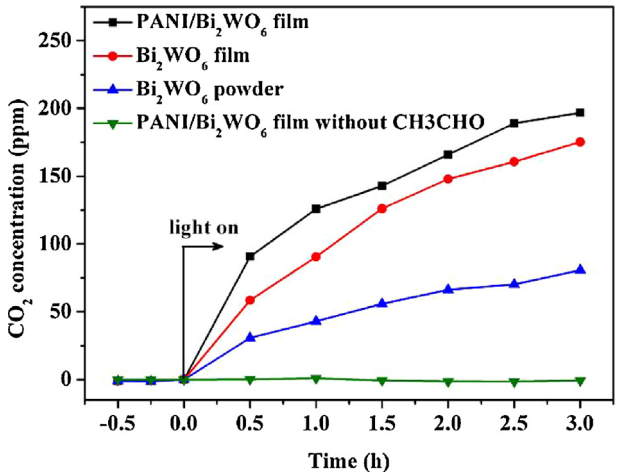


**Fig. 7.** Photocatalytic activity of PANI/$Bi_2WO_6$ film for the degradation of acetaldehyde (100 ppm) in air under visible light ($\lambda > 420$ nm).

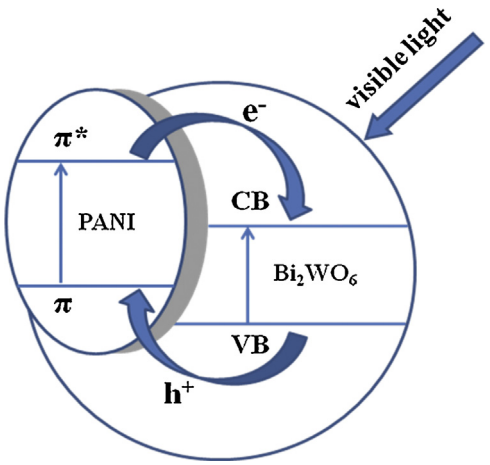


**Scheme 2.** Schematic diagram for energy band matching and migration and separation of electron–hole pairs in the coupled PANI/$Bi_2WO_6$ system.

does not absorb light; thus, the photosensitization process does not exist in such a photodegradation process. As shown in Fig. 7, $CH_3CHO$ was degraded by the $Bi_2WO_6$ and PANI/$Bi_2WO_6$ film with an obvious production of $CO_2$ under visible light irradiation. The PANI/$Bi_2WO_6$ film exhibited higher activity in the degradation of $CH_3CHO$ than pure $Bi_2WO_6$ film. For comparison, the photodegradation of $CH_3CHO$ by 0.05 g $Bi_2WO_6$ powders which were collected during CBD process was also tested. In gaseous system, the powders showed a comparatively low photocatalytic activity. After being irradiated for 3 h, $CH_3CHO$ was degraded almost completely by the PANI/$Bi_2WO_6$ film with the production of about 200 ppm $CO_2$, and nearly 80% of $CH_3CHO$ was degraded by pure $Bi_2WO_6$ film. However, the decomposition of $CH_3CHO$ by $Bi_2WO_6$ powders was less than 50% after the same irradiation time. The enhanced photocatalytic activity of the film compared with powders could be attributed to the new type of substrate. It increased the interface between the photocatalyst and contaminant because the photocatalyst particles were well dispersed on the substrate with high surface area, rather than agglomerated together in the static degradation system of catalyst powders. As a blank experiment, the PANI/$Bi_2WO_6$ film sample was irradiated under the same experimental condition without $CH_3CHO$ in the reactor. No production of $CO_2$ was detected, which indicated no photolysis of $CH_3CHO$ exists. Therefore, the degradation of $CH_3CHO$ was fully attributed to the photocatalytic process. Furthermore, the PANI/$Bi_2WO_6$ film did not produce any $CO_2$ itself under visible light irradiation, verifying stability of the PANI/$Bi_2WO_6$ film once again.

The above experiments have shown the excellent photocatalytic performance of the as-prepared PANI/$Bi_2WO_6$ on the degradation of the widely used dye and common indoor air pollutant. It follows that the PANI modified $Bi_2WO_6$ photocatalysis film may have highly potential applications in the conservation of the environment. Not only limited to the experimental results, the photodegraded mechanism of contaminants under visible light was necessary to investigate and guide the further improvement of its photocatalytic performance. The possible photocatalytic mechanism (Scheme 2) was proposed as follows:

$$\frac{Bi_2WO_6}{PANI} \xrightarrow{h\nu} h^+ + e^- \quad (1)$$

On the basis of the relative energy level of PANI ($\pi$-orbital and $\pi^*$-orbital) and $Bi_2WO_6$ (conduction band, CB, and valence band, VB) [29,30], the photogenerated holes in VB can directly transfer to the $\pi$-orbital of PANI. Simultaneously, the photogenerated electrons can transfer to the CB of $Bi_2WO_6$, which results in charge separation and stabilization, thus hindering the recombination process. PANI is a good material for transporting holes, and the grain size of the photocatalyst is also relatively small [31]; therefore, the photogenerated charges can emigrate to the surface of photocatalysts and photodegrade the adsorbed contaminations. With the synergic effect, the photocatalytic ability of PANI/$Bi_2WO_6$ film is improved remarkably. Further efforts are mainly focused on optimizing the content of coating PANI to improve the photocatalytic activity of PANI/$Bi_2WO_6$ film for practical application. Although the photocatalytic efficiency of the film is not comparable to that of the $Bi_2WO_6$ powders, the cost which is saved during the separation and recycling process makes this film promising for future environmental application, especially in the indoor air purification.

## 4. Conclusion

In conclusion, a CBD method was developed to deposit the $Bi_2WO_6$ photocatalyst on the reticular substrate of stainless steel mesh. The method involves mild temperatures and yields morphological well-defined $Bi_2WO_6$ nanoparticles. This coating process may be extended to the deposition of $Bi_2WO_6$ on various types of substrate and technological coating of other relevant photocatalysts. Compared to the slurry system, the photocatalytic activity of the as-prepared $Bi_2WO_6$ film decreased dramatically after immobilization, because of significant reduction of the interface between the photocatalyst and contaminant.

The photocatalytic activity of $Bi_2WO_6$ film was enhanced by the modification of PANI with intrinsic properties. The synergic effect between PANI and $Bi_2WO_6$ was realized through an in situ polymerization of aniline. The PANI/$Bi_2WO_6$ film exhibited efficient photocatalytic activity and excellent stability in oxidative decomposition of RhB under visible light ($\lambda > 420$ nm). In particular, the degradation of gaseous acetaldehyde eliminated the photosensitive effect of RhB, and verified the stability of the PANI/$Bi_2WO_6$ film once again. The excellent properties of the PANI/$Bi_2WO_6$ film were mainly ascribed to the rapid separation and slow recombination of the photogenerated electron–hole pairs. From the viewpoint of practical application, this work does not only solve the separation problem which is general for photocatalyst particles in slurry system, but also provided some insight into the design of photocatalysis film with high activity for environmental applications, especially the indoor air purification.

## Acknowledgment

This work is financially supported by the National Basic Research Program of China (2010CB933503, 2013CB933203) and National Natural Science Foundation of China (51272269, 51272303, and 51102262).

## References

[1] F. Amano, A. Yamakata, K. Nogami, M. Osawa, B. Ohtani, J. Am. Chem. Soc. 130 (2008) 17650.
[2] L. Ge, C.C. Han, J. Liu, Appl. Catal. B: Environ. 108 (2011) 100–107.
[3] X.C. Song, Y.F. Zheng, R. Ma, Y.Y. Zhang, H.Y. Yin, J. Hazard. Mater. 192 (2011) 186–191.
[4] Y. Tian, M. Fang, W. Xu, N.A. Li, Y.Z. Chen, L.D. Zhang, J. Nanosci. Nanotechnol. 11 (2011) 7802–7806.
[5] Z.J. Zhang, W.Z. Wang, E.P. Gao, M. Shang, J.H. Xu, J. Hazard. Mater. 196 (2011) 255–262.
[6] J.P. Li, X. Zhang, Z.H. Ai, F.L. Jia, L.Z. Zhang, J. Lin, J. Phys. Chem. C 111 (2007) 6832–6836.
[7] S.C. Zhang, J.D. Shen, H.B. Fu, W.Y. Dong, Z.J. Zheng, L.Y. Shi, J. Solid State Chem. 180 (2007) 1456–1463.
[8] X. Zhao, T.G. Xu, W.Q. Yao, C. Zhang, Y.F. Zhu, Appl. Catal. B: Environ. 72 (2007) 92–97.
[9] J.H. Xu, W.Z. Wang, M. Shang, S.M. Sun, J. Ren, L. Zhang, Appl. Catal. B: Environ. 93 (2010) 227–232.
[10] X.C. Wang, J.C. Yu, C.M. Ho, Y.D. Hou, X.Z. Fu, Langmuir 21 (2005) 2552–2559.
[11] S.B. Zhu, T.G. Xu, H.B. Fu, J.C. Zhao, Y.F. Zhu, Environ. Sci. Technol. 41 (2007) 6234–6239.
[12] S.E. Shaheen, C.J. Brabec, N.S. Sariciftci, F. Padinger, T. Fromherz, J.C. Hummelen, Appl. Phys. Lett. 78 (2001) 841–843.
[13] Y.J. Wang, J. Xu, W.Z. Zong, Y.F. Zhu, J. Solid State Chem. 184 (2011) 1433–1438.
[14] H. Zhang, R.L. Zong, Y.F. Zhu, J. Phys. Chem. C 113 (2009) 4605–4611.
[15] H. Zhang, R.L. Zong, J.C. Zhao, Y.F. Zhu, Environ. Sci. Technol. 42 (2008) 3803–3807.
[16] Y. Gao, Z.H. Kang, X. Li, X.J. Cui, J. Gong, CrystEngComm 13 (2011) 3370–3372.
[17] B.K. Gu, Y.A. Ismail, G.A. Spinks, S.I. Kim, I. So, S.J. Kim, Chem. Mater. 21 (2009) 511–515.
[18] J.Y. Lee, C.A. Bashur, A.S. Goldstein, C.E. Schmidt, Biomaterials 30 (2009) 4325–4335.
[19] A.A. Qaiser, M.M. Hyland, D.A. Patterson, J. Phys. Chem. B 113 (2009) 14986–14993.
[20] S. Bhadra, J.H. Lee, J. Appl. Polym. Sci. 114 (2009) 331–340.
[21] H.Y. Xu, H. Wang, T.N. Jin, H. Yan, Nanotechnology 16 (2005) 65–69.
[22] T.P. Niesen, M.R. De Guire, J. Electroceram. 6 (2001) 169–207.
[23] R. Zhang, L.L. Kerr, J. Solid State Chem. 180 (2007) 988–994.
[24] Y.S. Lo, R.K. Choubey, W.C. Yu, W.T. Hsu, C.W. Lan, Thin Solid Films 520 (2011) 217–223.
[25] X.H. Liu, M. Afzaal, T. Badcock, P. Dawson, P. O'Brien, Mater. Chem. Phys. 127 (2011) 174–178.
[26] T.S. Shyju, S. Anandhi, R. Indirajith, R. Gopalakrishnan, J. Alloys Compd. 506 (2010) 892–897.
[27] E. Matijevic, Annu. Rev. Mater. Sci. 15 (1985) 483–516.
[28] W. Zhao, C.C. Chen, X.Z. Li, J.C. Zhao, H. Hidaka, N. Serpone, J. Phys. Chem. B 106 (2002) 5022–5028.
[29] M.A. Butler, J. Appl. Phys. 48 (1977) 1914–1920.
[30] J. Li, L.H. Zhu, Y.H. Wu, Y. Harima, A.Q. Zhang, H.Q. Tang, Polymer 47 (2006) 7361–7367.
[31] Y. Shirota, H. Kageyama, Chem. Rev. 107 (2007) 953–1010.